Diffusion-Enhanced Hierarchically Macro-Mesoporous Catalyst for Selective Hydrogenation of Pyrolysis Gasoline

Zhiming Zhou, Tianying Zeng, Zhenmin Cheng, and Weikang Yuan
State Key Laboratory of Chemical Engineering, East China University of Science and Technology, Shanghai 200237, China

DOI 10.1002/aic.12421
Published online October 12, 2010 in Wiley Online Library (wileyonlinelibrary.com).

A novel Pd/Al_2O_3 catalyst with the hierarchically macro-mesoporous structure was prepared and applied to the selective hydrogenation of pyrolysis gasoline. The alumina support possessed a unique structure of hierarchical mesopores and macropores. The as-prepared and calcined alumina were characterized by X-ray diffraction, N_2 adsorption-desorption, and scanning electron microscopy. It showed that the hierarchically porous structure of the alumina was well preserved after calcination at 1073 K, indicating high thermal stability. The 1073 K calcined alumina was impregnated with palladium metal and compared with a commercial catalyst without macrochannels. Both the catalytic activity and the hydrogenation selectivity of the novel Pd/Al_2O_3 catalyst were higher than those of the commercial Pd/Al_2O_3 catalyst. In addition, apparent reaction activation energies obtained with the novel catalyst for model pyrolysis gasoline were 46–81% higher than those with the commercial catalyst. The results adequately demonstrated the enhanced mass transfer characteristics of the novel macro-mesostructured catalyst. © 2010 American Institute of Chemical Engineers *AIChE J,* 57: 2198–2206, 2011

Keywords: catalysis, diffusion, hierarchically macro-mesoporous alumina, selective hydrogenation, pyrolysis gasoline

Introduction

Pyrolysis gasoline (pygas), a byproduct of steam cracking of naphtha, contains a large quantity of aromatic compounds, such as benzene, toluene, and xylene, and a small amount of unsaturated compounds such as olefins and diolefins.[1,2] The huge amount of pygas produced annually in petrochemical plants and the high percentage of aromatics involved make pygas a potential feedstock for aromatics production. Selective hydrogenation of pygas plays a very important role in the post-treatment of pygas, which aims at converting about 90% of styrene and diolefins into ethylbenzene and monoolefins, respectively, and meanwhile, only less than 10% of monoolefins are hydrogenated into saturates.[3,4]

Among various components involved in pygas, styrene and diolefins are so unstable that they are subject to polymerization through the double bond, which consequently results in gum formation.[5,6] These gums will probably cover some metal active sites of the catalyst and block some mesopores. As a result, catalyst deactivation will take place. The strategy to prevent gum formation is to reduce the residence time of diolefins inside the catalyst, in another word, to reduce the internal diffusion limitations of diolefins.

In previous work on a commercial catalyst[7] for selective hydrogenation of pygas,[8] we found that the pore-size distribution of the commercial catalyst (4–20 nm) was not

Correspondence concerning this article should be addressed to Z. Zhou at zmzhou@ecust.edu.cn.

suitable for the present reaction system from the viewpoint of long-term operation because of the heavy internal diffusion limitations of reactants. To reduce the internal diffusion resistance, a novel catalyst support with a hierarchically macro-mesoporous structure was prepared and applied to selective hydrogenation of pygas in another previous work.[9] In that work, a preliminary test performed at a given temperature (313 K) and pressure (2.0 MPa) showed that the hierarchically porous catalyst exhibited higher activity and selectivity than the commercial catalyst. However, this result was not so convincing considering that only one reaction test was conducted with the novel catalyst.

In fact, hierarchically macro-mesoporous metal oxides have recently attracted considerable attention because of their potential applications.[10,11] Their unique pore structures, i.e., the monolithic macropores and the accessible mesopores, make them high-potential supports and catalysts.[12] Application examples include oxidation[13–17] and hydrogenation reactions.[9,18] Wang et al.[13,14] and Yu et al.[15] prepared hierarchically macro-mesoporous TiO_2 for photocatalytic oxidation decomposition of volatile organic compounds. Tidahy et al.[16] made use of hierarchically porous ZrO_2[19,20] as catalyst support for VOCs catalytic oxidation. Cao et al.[17] synthesized hierarchically macro-mesoporous TiO_2-supported CuO catalysts for CO oxidation. Our group prepared hierarchically porous Pd/TiO_2 and Pd/Al_2O_3 catalysts for hydrogenation of styrene[18] and selective hydrogenation of pygas,[9] respectively. All these investigations reported that the uniquely bidisperse pore structure could enhance catalytic activities through improved mass transfer. However, in these studies, only few comparisons were made between the hierarchically porous catalysts and the normal catalysts, and no systematic investigation was carried out to testify the enhanced mass transfer characteristics of the novel structured catalysts.

As a part of a series of studies on selective hydrogenation of pygas, the main aim of this work is to adequately verify the diffusion-enhanced effect of the hierarchically macro-mesoporous structure of the novel Pd/Al_2O_3 catalyst. Different from our previous work,[9] more detailed characterizations on the support and the catalyst are conducted in this article, and more important, the apparent reaction kinetics of selective hydrogenation of pygas over the novel Pd/Al_2O_3 catalyst is investigated, and the results are compared with those obtained with the commercial catalyst.

Experimental

Preparation of support and catalyst

Detailed information about preparation of the catalyst support, namely the hierarchically macro-mesoporous alumina, and the corresponding palladium-supported catalysts was presented elsewhere.[9,21,22] The hierarchically porous aluminum oxide used in this work was prepared with the aid of surfactant (cetyltrimethylammonium bromide, CTAB) under the following conditions: 2 g of aluminum tri-*sec*-butoxide, 35 mL of twice-distilled water, 15 mL of absolute ethanol, and 0.4 g of CTAB, pH 12, 350 rpm, room temperature, and 1 h of reaction. The 1073 K calcined alumina with the hierarchically porous structure was sieved to a diameter range of 50–75 μm and used as catalyst support. The palladium-supported catalyst with 0.3 wt % (mass percent) metal loading was finally prepared by incipient-wetness impregnation of the aforementioned support with palladium chloride aqueous solution. For comparison, the commercial catalyst, supplied by the Chemical Research Institute of Lanzhou Petrochemical Corporation, was also ground and sieved to 50–75 μm for the kinetic study.

Characterization

X-ray diffraction (XRD) patterns of the prepared samples were obtained on a Rigaku D/Max 2550 VB/PC diffractometer with Cu Kα radiation scanning 2θ angles ranging from 10° to 80°. Nitrogen adsorption-desorption isotherms and the corresponding pore-size distributions were acquired at 77 K on a Micromeritics ASAP 2010 instrument. All the samples were degassed at 463 K and 1 mm Hg for 6 h before nitrogen adsorption measurements. The pore diameter and the pore-size distribution were determined by the BJH method. The morphology and the macroporous array of the Al_2O_3 powders were examined with a JEOL JSM 6360 LV scanning electron microscope (SEM). High-resolution transmission electron microscopy (HRTEM) investigation was performed using a JEOL JEM-2010 transmission electron microscope. The samples prepared for HRTEM investigation were first dispersed in ethanol under ultrasound and then a drop of the sample–ethanol solution was transferred onto a carbon-coated copper grid. Metal dispersions were measured by using CO pulse chemisorption on a Micromeritics AutoChem 2920 apparatus. The weighed catalysts were reduced in a mixture of 10% H_2/Ar (100 ml/min) at 423 K for 2 h followed by a switch to helium (100 ml/min) at 463 K for 20 min to remove adsorbed hydrogen. After the catalysts were cooled to 308 K in a helium flow, carbon monoxide pulses were injected into the quartz reactor, and the net volume of CO was monitored with a thermal conductivity detector. For Pd/Al_2O_3 catalysts with palladium chloride as the precursor, the mean stoichiometry of palladium metal to CO molecule can be taken as 1 according to the data summarized by Joyal and Butt.[23]

Selective hydrogenation of pygas

Hydrogenation of a model pygas feed, which was composed of styrene, cyclopentadiene, 1-hexene, and *n*-heptane (solvent), was carried out in a stirred autoclave at total pressures of 2.0–4.0 MPa over a temperature range of 303–343 K. During each run, the autoclave was first heated to the desired temperature under N_2 protection, and then, it was purged with preheated hydrogen for five times to exclude N_2. The autoclave was operated in a semibatch mode with hydrogen continuously entering into the autoclave to maintain the pressure. The temperature was controlled within $\pm$0.5 K of the desired value and the pressure within $\pm$0.02 MPa. Liquid samples were collected for analysis at different time points.

A preliminary test on the effect of the stirring speed on the reaction rate of styrene hydrogenation showed that the stirring speed had no effect on the reaction rate when it was above 800 rpm, implying the elimination of the external

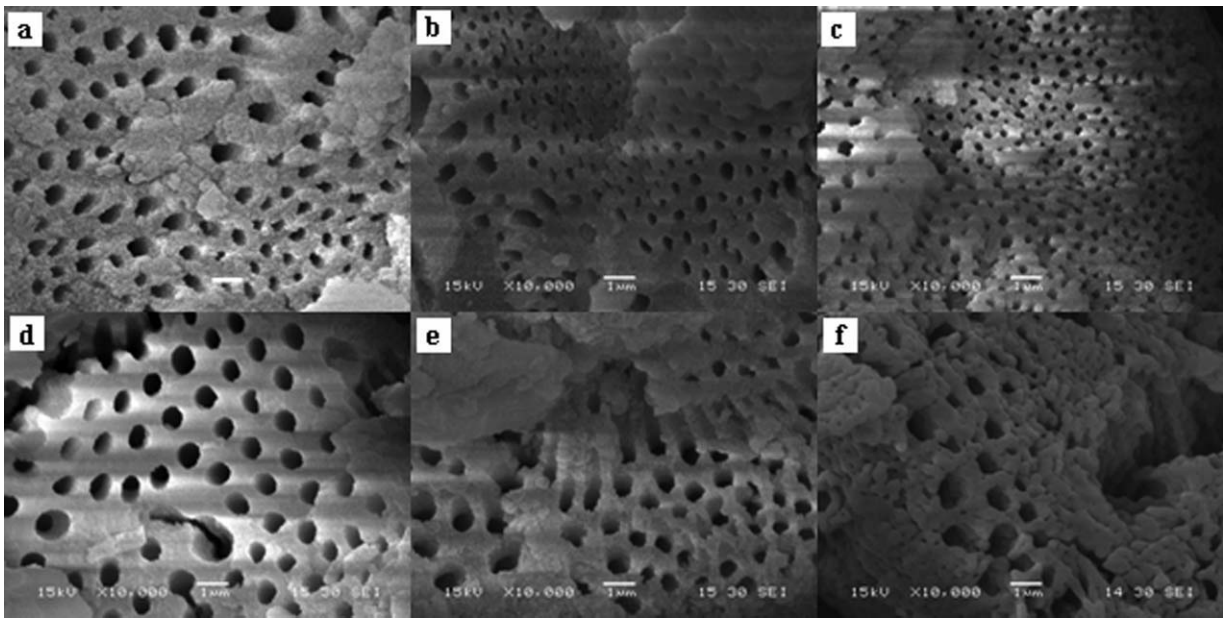

Figure 1. SEM images of (a) the prepared macro-mesoporous aluminum oxide and the calcined alumina at different temperatures; (b) 473 K, (c) 673 K, (d) 873 K, (e) 1073 K, and (f) 1273 K.

Scale bar: 1 μm.

mass transfer limitation. In this work, all the kinetic experiments were carried out at a stirring speed of 1000 rpm.

Four reaction classes were concerned with the selective hydrogenation of the model pygas, i.e.,

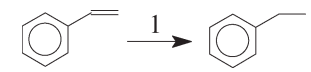

(1)

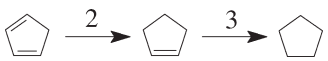

(2)

(3)

Styrene (STY) and 1-hexene (HEX) were hydrogenated to ethylbenzene and *n*-hexane, respectively. Cyclopentadiene (CPD) was hydrogenated to cyclopentene (CPE), which was further hydrogenated to cyclopentane (CPA).

Analytical method

The liquid samples were analyzed with a Hewlett-Packard 6890 gas chromatograph equipped with a flame ionization detector. A HP-5 capillary column (30 m $\times$ 0.32 mm $\times$ 0.25 μm) was used for separation. *n*-Octane was used as the internal standard. The oven temperature program consisted of the following segments: start at 318 K (hold for 3 min), ramp at 15 K/min to 493 K, and finally hold at 493 K for 2 min. The temperatures at the injector and the detector were set at 493 and 523 K, respectively.

Results and Discussion

Physicochemical characterization

Figure 1 shows the SEM images of the prepared aluminum oxides and the calcined alumina at different temperatures. Apparently, the macroporous channels inside the alumina are parallel to each other and perpendicular to the tangent of the outer surface. For those alumina samples calcined at a temperature range of 473–1073 K (Figures 1b–e), the macroporous structures are well preserved, and the macropore size as well as the wall thickness has less change, which indicates good thermal stability of the hierarchically porous alumina. When the calcination temperature is further up to 1273 K (Figure 1f), although wall collapse occurrs in some regions, the macroporous structure is partly preserved. The formation of the hierarchically porous structure can be explained by a spontaneous self-assembly mechanism, which is presented elsewhere.[9,12,24–26]

Figure 2 presents the XRD patterns of the prepared and the calcined alumina. The as-prepared sample (Figure 2a) and the calcined product at 473 K (Figure 2b) exhibit diffraction peaks assigned to the boehmite phase AlOOH (JCPDS 21-1307). When the sample is calcined at 673 K (Figure 2c) and 873 K (Figure 2d), γ-Al_2O_3 phase (JCPDS 10-0425) is formed as a result of the dehydration of alumina oxyhydroxide boehmite.[27] With a further increase in the temperature to 1073 K (Figure 2e), the γ-Al_2O_3 phase transforms to δ-Al_2O_3 (JCPDS 16-0394). When the sample is calcined up to 1273 K (Figure 2f), the α-Al_2O_3 phase (JCPDS 10-0173) is observed.

The N_2 adsorption-desorption isotherms of the above samples (a–f) and the pore-size distribution curves are shown in Figure 3. The textural properties of these samples are reported in Table 1. Except for the 1273 K calcined sample, all the other isotherms of the calcined samples (b–e) are of

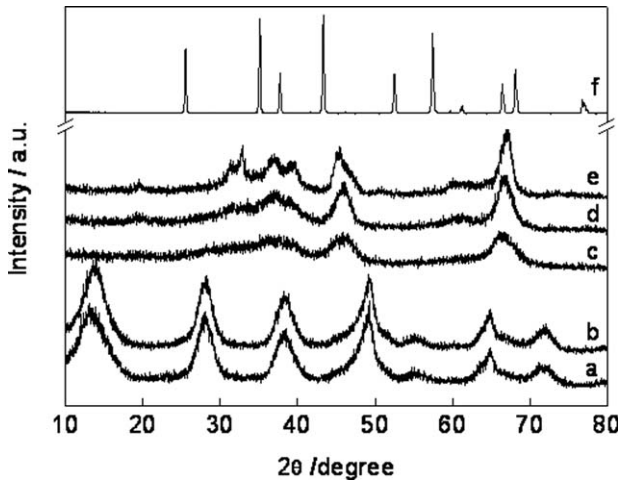

Figure 2. X-ray diffraction patterns of (a) the prepared macro-mesoporous aluminum oxide and the calcined alumina at different temperatures; (b) 473 K, (c) 673 K, (d) 873 K, (e) 1073 K, and (f) 1273 K.

type IV with a hysteresis loop, indicating that the mesopore network is still sustained after high temperature treatment. Under calcination at 1273 K, the sample shows a nonporous structure, indicating collapse of the mesopores. Sample g listed in Table 1 is a commercial Pd/δ-Al_2O_3 catalyst for selective hydrogenation of pygas, and this catalyst has no macroporous channels.[7,9]

Except for the macroporous structure, the textural properties of the commercial catalyst are similar to those of sample e, i.e., the 1073 K calcined Al_2O_3, and both of them exhibit the same crystalline phase, i.e., the δ-Al_2O_3 phase. In addition, as shown in Figure 4, the pore-size distribution curves of these two catalysts almost overlap. As a result, the 1073 K calcined Al_2O_3 is selected to be the support for the novel catalyst. For simplicity, the novel catalyst with the hierarchically macro-mesoporous structure and the commercial catalyst are denoted by Pd/Al_2O_3(novel) and Pd/Al_2O_3(com), respectively.

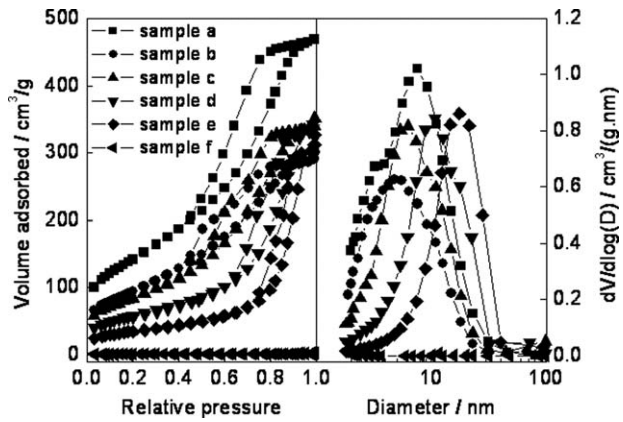

Figure 3. N_2 adsorption-desorption isotherms and the pore-size distribution curves of the as-prepared and the calcined alumina samples.

Table 1. Textural Properties of the As-Prepared and the Calcined Alumina Samples

No	S_{BET} (m^2/g)	Pore Volume (cm^3/g)	Macropore Size* (μm)	Mesopore Size† (nm)
a	514.1	0.81	0.45	5.9
b	341.4	0.49	0.40	5.0
c	309.0	0.56	0.45	6.0
d	211.1	0.64	0.55	10.7
e	126.4	0.51	0.45	14.3
f	3.8	–	0.70	–
g‡	98.1	0.37	–	14.9

*The average macropore diameter is obtained from analysis of the image.
†BJH pore diameter is determined from the adsorption branch.
‡The commercial Pd/δ-Al_2O_3 catalyst.

Values of palladium dispersion obtained from CO chemisorption are 32.5 and 29.6% for Pd/Al_2O_3(novel) and Pd/Al_2O_3(com), respectively. Based on the dispersion values (D), the mean palladium particle size (d_P) is calculated from the following equation[28]

$$d_P = \frac{112}{D(\%)}. \tag{4}$$

The mean palladium particle sizes of Pd/Al_2O_3(novel) and Pd/Al_2O_3(com) catalysts are almost the same, being 3.4 and 3.8 nm, respectively.

Figure 5 shows the HRTEM images of the novel catalyst. The metallic particles indicated by arrow are palladium metal according to the energy-dispersive X-ray analysis. The palladium particle size determined by HRTEM is about 3.6 nm, which is consistent with that obtained from the CO chemisorption measurement.

Catalytic activity

Figure 6 presents concentration variations of various species over Pd/Al_2O_3(novel) and Pd/Al_2O_3(com) catalysts. It is evident that the novel catalyst exhibits much higher catalytic activity than the commercial catalyst. Taking the reaction occurring at 313 K and 3.0 MPa as an example (Figure 6A), the time needed for complete conversion of cyclopentadiene

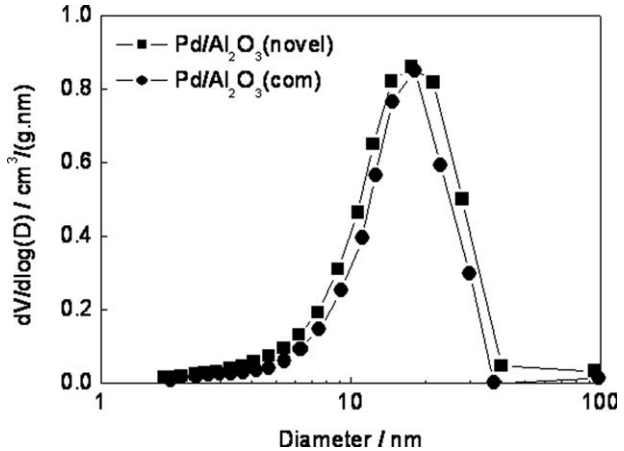

Figure 4. Pore-size distribution curves of the novel and the commercial catalysts.

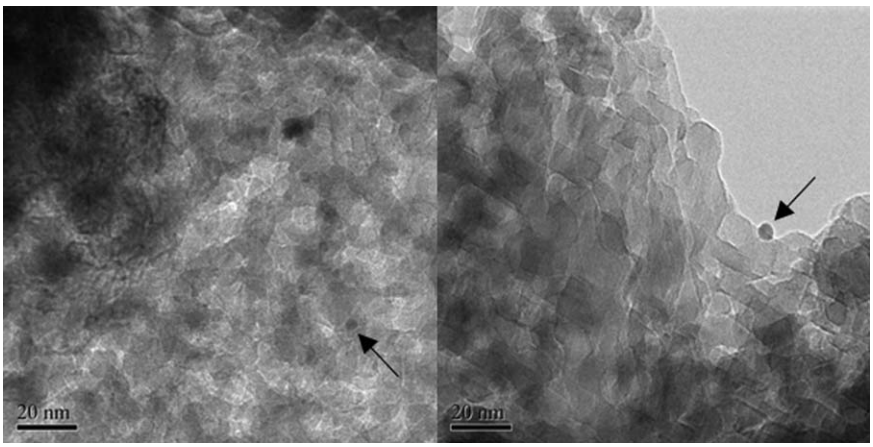

Figure 5. HRTEM images of the Pd/Al_2O_3(novel) catalyst.

Scale bar: 20 nm.

and styrene over the Pd/Al_2O_3(novel) catalyst is only 15 min, but it is about 40 min for the Pd/Al_2O_3(com) catalyst.

Further observation of Figure 6A shows that in the first 9 min of reaction over the Pd/Al_2O_3(novel) catalyst, most cyclopentadiene is conversed to cyclopentene and styrene is partly reacted, whereas 1-hexene and cyclopentene are hardly consumed. Only when cyclopentadiene and styrene are hydrogenated to a great extent do 1-hexene and cyclopentene have an obvious conversion. It implies that high selectivity of diolefin hydrogenation to monoolefin can be obtained over the novel catalyst.

To clarify which catalyst possesses the higher hydrogenation selectivity, two parameters are defined as follows:

$$S_1 = \frac{\text{Conversion of } 1-\text{hexene}}{\text{Conversion of cyclopentadiene}} \times 100\% \qquad (5)$$

$$S_2 = \frac{\text{Conversion of } 1-\text{hexene}}{\text{Conversion of styrene}} \times 100\%. \qquad (6)$$

Obviously, the smaller S_1 and S_2, the higher the selectivity of diolefins to monoolefins. As shown in Figure 7, the Pd/Al_2O_3(novel) catalyst exhibits the higher hydrogenation selectivity in terms of both cyclopentadiene and styrene. The X-axis in Figure 7, α_{CPD} and α_{STY}, represent conversions of cyclopentadiene and styrene, respectively.

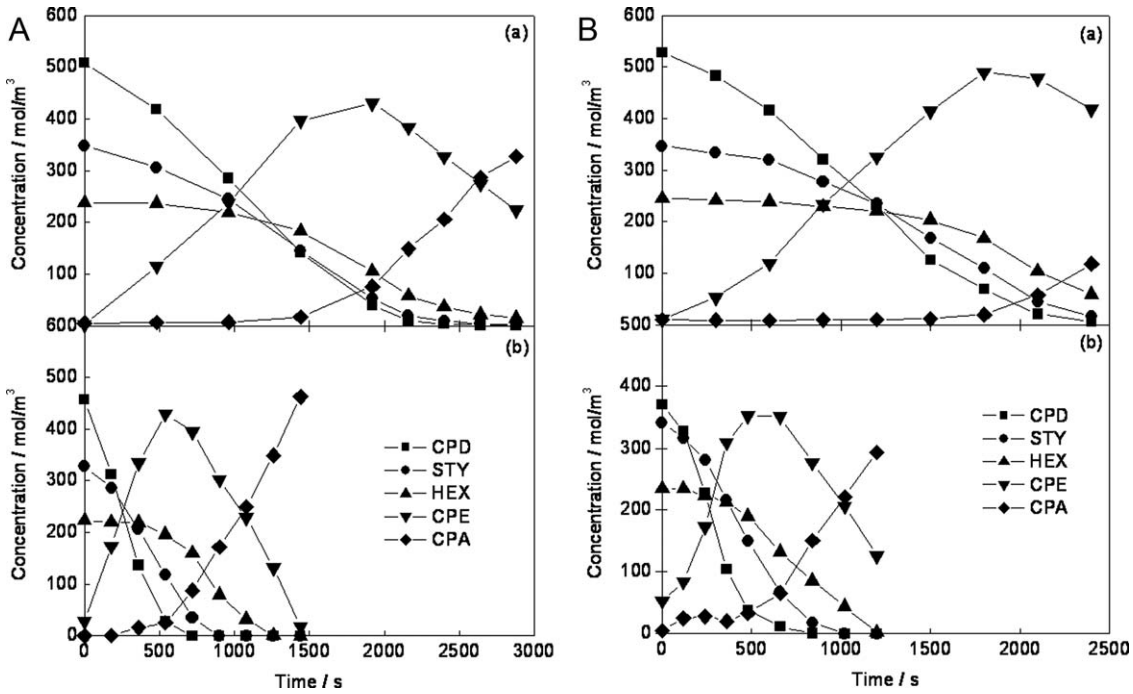

Figure 6. Concentration–time profiles for various species over (a) the commercial catalyst and (b) the novel catalyst.

Reaction conditions: (A) $T = 313$ K, $P = 3.0$ MPa; (B) $T = 323$ K, $P = 2.0$ MPa.

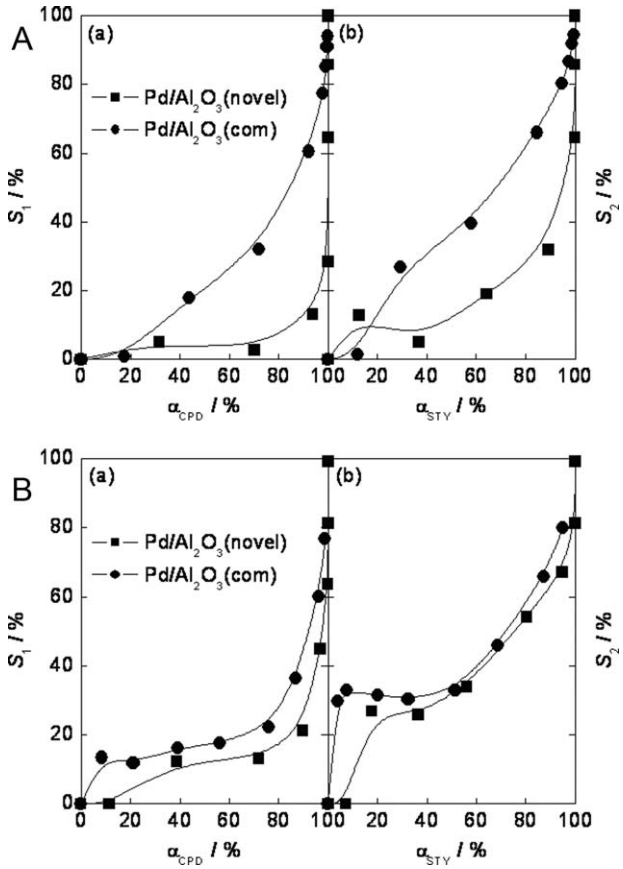

Figure 7. Hydrogenation selectivity of different catalysts based on (a) cyclopentadiene and (b) styrene.

Reaction conditions: (A) $T = 313$ K, $P = 3.0$ MPa; (B) $T = 323$ K, $P = 2.0$ MPa.

The above analyses of the activity and the selectivity of the two catalysts reveal that the novel catalyst has better catalytic performance than the commercial catalyst for the reaction system of selective hydrogenation of pygas. The main reasons lie in three aspects. First, the diffusion resistance of reactants from the outer surface to the inner surface of the catalyst can be greatly reduced in the monolithic macroporous channels.[29–31] For the catalysts with a large-pore structure, previous studies also showed that the effectiveness factors could be increased to some extent as a result of the enhancement of the effective diffusivity because of the existence of the intraparticle convection.[32–35] Second, the narrow walls separating the macropores can shorten the diffusion distance of reactants to the active sites and consequently decrease the concentration gradient of species, which in turn increases the reaction rate; third, both macroporous channels and narrow walls can reduce the residence time of the intermediate products (monoolefins) inside the catalyst and prevent further hydrogenation of monoolefins to saturated hydrocarbons, which is favorable for the high selectivity of diolefins to monoolefins.

To further testify the advantage of the hierarchically macro-mesoporous structure of the novel catalyst in reducing the internal diffusion limitations, the apparent reaction kinetics of selective hydrogenation of pygas over the novel catalyst is investigated, and the kinetic parameters obtained with the novel catalyst and with the commercial catalyst are compared.

Reaction Kinetics

The apparent kinetics of selective hydrogenation of pygas over the commercial catalyst has been systematically investigated in our previous work.[3,8] Here, we use the same kinetic model to describe the reaction system over the novel catalyst. Detailed information about the development of the kinetic model is reported elsewhere.[3] The rate expressions for reactions (Eqs. 1–3) are given by

$$\frac{dc_{\mathrm{STY}}}{dt} = -\frac{m}{V}\cdot\frac{k_1 b_{\mathrm{STY}} c_{\mathrm{STY}}\sqrt{b_{\mathrm{H}}c_{\mathrm{H}}}}{A_1 A_2} \tag{7}$$

$$\frac{dc_{\mathrm{CPD}}}{dt} = -\frac{m}{V}\cdot\frac{k_2 b_{\mathrm{CPD}} c_{\mathrm{CPD}}\sqrt{b_{\mathrm{H}}c_{\mathrm{H}}}}{A_1 A_2} \tag{8}$$

$$\frac{dc_{\mathrm{CPE}}}{dt} = \frac{m}{V}\left(\frac{k_2 b_{\mathrm{CPD}} c_{\mathrm{CPD}}\sqrt{b_{\mathrm{H}}c_{\mathrm{H}}}}{A_1 A_2} - \frac{k_3 b_{\mathrm{CPE}} c_{\mathrm{CPE}}\sqrt{b_{\mathrm{H}}c_{\mathrm{H}}}}{A_1 A_2}\right) \tag{9}$$

$$\frac{dc_{\mathrm{HEX}}}{dt} = -\frac{m}{V}\cdot\frac{k_4 b_{\mathrm{HEX}} c_{\mathrm{HEX}}\sqrt{b_{\mathrm{H}}c_{\mathrm{H}}}}{A_1 A_2}, \tag{10}$$

where c is the molar concentration of reactant, t is the reaction time, m is the catalyst mass, V is the liquid volume, k_i is the rate constant of the ith reaction, and b_j is the adsorption constant of species j. A_1 and A_2 in the denominator of Eqs. 7–10 are equal to $1 + \sqrt{b_{\mathrm{H}}c_{\mathrm{H}}}$ and $1 + \sum b_j c_j$ (j = STY, CPD, CPE, and HEX), respectively. The temperature dependences of rate constants and adsorption constants can be expressed by

Table 2. Estimated Kinetic and Adsorption Parameters for Pd/Al_2O_3(com) and Pd/Al_2O_3(novel) Catalysts

	Preexponential Factor*		Apparent Activation Energy†	
Parameter	Pd/Al_2O_3(com)	Pd/Al_2O_3(novel)	Pd/Al_2O_3(com)	Pd/Al_2O_3(novel)
k_1	1.06×10^9	4.67×10^9	28.56	43.84
k_2	1.37×10^6	1.41×10^8	24.37	43.60
k_3	5.45×10^8	1.12×10^9	37.54	54.69
k_4	4.37×10^8	1.06×10^{10}	31.18	56.55
b_{STY}	3.67×10^{-4}	2.81×10^{-4}	12.35	11.83
b_{CPD}	2.06×10^{-3}	1.79×10^{-3}	19.32	17.61
b_{CPE}	1.53×10^{-4}	2.16×10^{-4}	10.81	20.76
b_{HEX}	2.19×10^{-4}	3.14×10^{-4}	12.59	17.67
b_{H}	2.39×10^{-8}	2.74×10^{-8}	14.63	16.19

*The units for k_i and b_j are mol/(kg s) and m^3/mol, respectively.
†The unit for activation energy is kJ/mol.

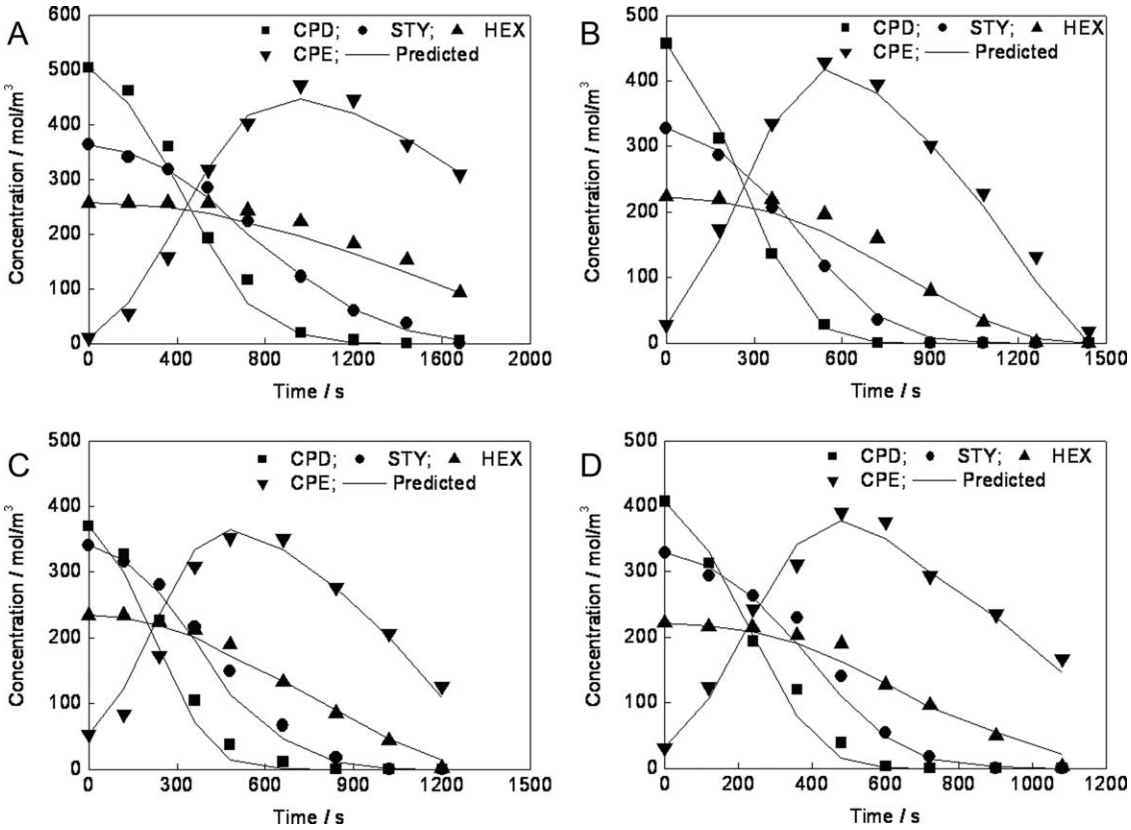

Figure 8. Experimental and predicted concentration–time profiles over the Pd/Al_2O_3(novel) catalyst (points: experimental; lines: predicted).

Reaction conditions: (A) $T = 303$ K, $P = 2.0$ MPa; (B) $T = 313$ K, $P = 3.0$ MPa; (C) $T = 323$ K, $P = 2.0$ MPa; and (D) $T = 333$ K, $P = 2.0$ MPa.

$$k_i = k_i^0 \exp[-E_i/(R_g T)], \quad i = 1, 2, 3, 4 \tag{11}$$

$$b_j = b_j^0 \exp[Q_j/(R_g T)], \quad j = \text{STY, CPD, CPE, HEX, H} \tag{12}$$

where k_i^0 is the preexponential factor of the rate constant of the ith reaction, b_j^0 is the preexponential factor of the adsorption constant of species j, E_i is the activation energy of the ith reaction, Q_j is the adsorption activation energy of species j, R_g is the universal gas constant, and T is the reaction temperature.

There are 18 kinetic and adsorption parameters in the kinetic model (Eqs. 7–12), which can be estimated by fitting all the experimental data. The optimized values of these parameters are determined by using the Rosenbrock algorithm,[36] which minimizes the residual sum of squares between the experimental and the calculated concentrations of all reactants. The ordinary differential equations involved in the kinetic model are integrated by the DASSL solver.[37,38]

The estimated values of the 18 parameters for the novel and the commercial catalysts are summarized in Table 2. The apparent activation energies of all the four reactions (Eqs. 1–3) obtained with the novel catalyst are higher than those with the commercial catalyst, the former being 46–81% higher than the latter. This result, on one hand, indicates the heavy internal diffusion limitations of species in the commercial catalyst[39] and, on the other hand, proves that the hierarchically macro-mesoporous structure does greatly reduce the influence of internal diffusion resistance.

The existence of internal mass transfer limitation in the commercial Pd/Al_2O_3(com) catalyst can be verified by calculating from the observed reaction rate the Weisz-Prater parameter,[39,40] Φ_{H_2}, as

$$\Phi_{H_2} = \left(\eta\varphi^2\right)_{H_2} = \frac{r_H \rho_C d_P^2}{36 c_H W_S \rho_L D_{e,H}}, \tag{13}$$

where r_H is the observed reaction rate of hydrogen, ρ_C is the density of the catalyst, d_P is the diameter of the catalyst particle, W_S is the catalyst weight fraction in the liquid, ρ_L is the density of the liquid, and $D_{e,H}$ is the effective diffusivity of hydrogen. Corresponding to the reactions occurring at 313, 323, 333, and 343 K (the pressure is 2.0 MPa), the estimated Weisz-Prater parameters are 1.34, 1.45, 1.61, and 1.89, respectively. All the values are greater than 1, indicating the presence of intraparticle diffusion in the commercial catalyst.

The estimated apparent activation energy for styrene hydrogenation over the commercial catalyst in this work, 28.56 kJ/mol, is very close to that reported by Nijhuis et al.,[5] 27 kJ/mol. Nijhuis et al.[5] used a commercial catalyst with the diameter of 40–100 μm to study the reaction kinetics of styrene hydrogenation. By comparison with the values reported by Chaudhari et al.[41] (55 kJ/mol) and by Jackson and Shaw[42] (41 $\pm$ 8 kJ/mol), they found that the obtained

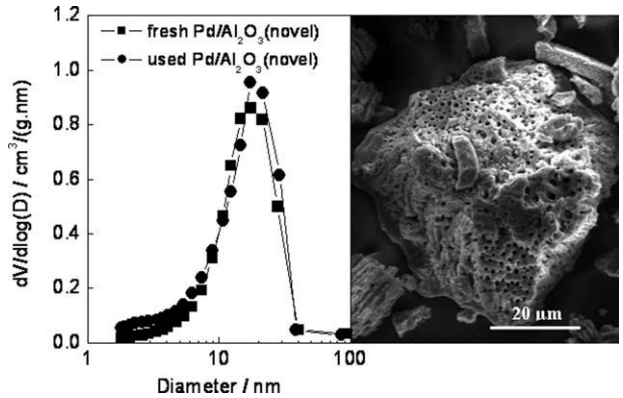

Figure 9. Pore-size distribution curves of fresh and used Pd/Al_2O_3(novel) catalysts as well as the SEM image of the used catalyst.

activation energy of 27 kJ/mol was greatly influenced by internal mass transfer effects. On the other hand, for the novel hierarchically structured catalyst, the apparent activation energy amounts to 43.84 kJ/mol, which is in good agreement with that reported by Jackson and Shaw.[42] Therefore, the above analysis further supports that the intraparticle diffusion resistance of the novel catalyst is much smaller than that of the commercial catalyst.

Typical results of experimental and predicted concentration–time profiles for various species over the Pd/Al_2O_3(novel) catalyst are shown in Figure 8. The agreement between the experimental and the predicted data is observed to be very well for each species, indicating the reliability and accuracy of the kinetic model to describe the reaction system of selective hydrogenation of pygas.

After the kinetic investigation, the Pd/Al_2O_3(novel) catalyst is recovered and analyzed. As shown in Figure 9, the pore-size distribution of the used Pd/Al_2O_3(novel) catalyst is almost the same as that of the fresh catalyst. In addition, the macrochannels are still well preserved. Neither wall collapse nor macropore blockage is observed through SEM images. Therefore, the hierarchically macro-mesoporous structure of the novel catalyst is very stable and resistant to the reaction environment of selective hydrogenation of pygas.

Conclusions

Hierarchically macro-mesoporous alumina was prepared by hydrolysis and condensation of the aluminum alkoxide precursor in an aqueous solution. After calcination of the prepared aluminum oxide from 473 K up to 1073 K, the monolithic macropores were well preserved, indicating the high thermal stability of the alumina. A novel palladium catalyst supported on the 1073 K calcined alumina was then prepared and applied to selective hydrogenation of pygas. By comparison with a commercial catalyst, the novel catalyst exhibited much higher activity and selectivity for pygas hydrogenation under various reaction conditions, which was mainly ascribed to the hierarchically porous structure of the novel catalyst. Apparent activation energies obtained with the novel catalyst for the model pygas were 46–81% higher than those with the commercial catalyst, which further manifested the advantage of the hierarchically macro-mesoporous structure in enhancing the mass transfer of components within the catalyst. Comparison of the fresh and the used catalysts demonstrated the good stability of the novel catalyst.

Acknowledgments

The authors thank the National Natural Science Foundation of China (No. 20706018), the National High Technology Research and Development Program of China (No. 2008AA05Z405), the Program for Changjiang Scholars and Innovative Research Team in University (No. IRT0721), and the "111" Project (No. B08021) for financial support of this work.

Literature Cited

1. Zhou ZM, Cheng ZM, Yang D, Zhou X, Yuan WK. Solubility of hydrogen in pyrolysis gasoline. *J Chem Eng Data*. 2006;51:972–976.
2. Mostoufi N, Sotudeh-Gharebagh R, Ahmadpour M, Eyvani J. Simulation of an industrial pyrolysis gasoline hydrogenation unit. *Chem Eng Technol*. 2005;28:174–181.
3. Zhou ZM, Cheng ZM, Cao YN, Zhang JC, Yang D, Yuan WK. Kinetics of the selective hydrogenation of pyrolysis gasoline. *Chem Eng Technol*. 2007;30:105–111.
4. Yang D, Cheng ZM, Zhou ZM, Zhang JC, Yuan WK. Pyrolysis gasoline hydrogenation in the second-stage reactor: reaction kinetics and reactor simulation. *Ind Eng Chem Res*. 2008;47:1051–1057.
5. Nijhuis TA, Dautzenberg FM, Moulijn JA. Modeling of monolithic and trickle-bed reactors for the hydrogenation of styrene. *Chem Eng Sci*. 2003;58:1113–1124.
6. Kaminsky MP. Pyrolysis gasoline stabilization. US Patent 6,949,686, 2005.
7. Li SQ, Men XT, Liu GS, Liang SQ, Zhang XG. Selective hydrogenation catalyst for pyrolysis gasoline. US Patent 6,576,586, 2003.
8. Zhou ZM, Zeng TY, Cheng ZM, Yuan WK. Kinetics of selective hydrogenation of pyrolysis gasoline over an egg-shell catalyst. *Chem Eng Sci*. 2010;65:1832–1839.
9. Zhou ZM, Zeng TY, Cheng ZM, Yuan WK. Preparation of a catalyst for selective hydrogenation of pyrolysis gasoline. *Ind Eng Chem Res*. 2010;49:1112–1118.
10. Su BL, Léonard A, Yuan ZY. Highly ordered mesoporous CMI-n materials and hierarchically structured meso-macroporous compositions. *C R Chimie*. 2005;8:713–726.
11. Yang XY, Li Y, Lemaire A, Yu JG, Su BL. Hierarchically structured functional materials: synthesis strategies for multimodal porous networks. *Pure Appl Chem*. 2009;81:2265–2307.
12. Vantomme A, Léonard A, Yuan ZY, Su BL. Self-formation of hierarchical micro-meso-macroporous structures: generation of the new concept "hierarchical catalysis". *Colloids and Surf A: Physicochem Eng Aspects*. 2007;300:70–78.
13. Wang XC, Yu JC, Ho CM, Hou YD, Fu XZ. Photocatalytic activity of a hierarchically macro/mesoporous titania. *Langmuir*. 2005;21:2552–2559.
14. Chen XF, Wang XC, Fu XZ. Hierarchical macro/mesoporous TiO_2/SiO_2 and TiO_2/ZrO_2 nanocomposites for environmental photocatalysis. *Energy Environ Sci*. 2009;2:872–877.
15. Yu JG, Su YR, Cheng B. Template-free fabrication and enhanced photocatalytic activity of hierarchical macro-/mesoporous titania. *Adv Funct Mater*. 2007;17:1984–1990.
16. Tidahy HL, Hosseni M, Siffert S, Cousin R, Lamonier JF, Aboukaïs A, Su BL, Giraudon JM, Leclercq G. Nanostructured macro-mesoporous zirconia impregnated by noble metal for catalytic total oxidation of toluene. *Catal Today*. 2008;137:335–339.
17. Cao JL, Shao GS, Ma TY, Wang Y, Ren TZ, Wu SH, Yuan ZY. Hierarchical meso-macroporous titania-supported CuO nanocatalysts: preparation, characterization and catalytic CO oxidation. *J Mater Sci*. 2009;44:6717–6726.
18. Zeng TY, Zhou ZM, Zhu J, Cheng ZM, Yuan PQ, Yuan WK. Palladium supported on hierarchically macro-mesoporous titania for styrene hydrogenation. *Catal Today*. 2009;147S:41–45.

19. Yuan ZY, Vantomme A, Léonard A, Su BL. Surfactant-assisted synthesis of unprecedented hierarchical meso-macrostructured zirconia. *Chem Commun.*2003;1558–1559.
20. Blin JL, Léonard A, Yuan ZY, Gigot L, Vantomme A, Cheetham AK, Su BL. Hierarchically mesoporous/macroporous metal oxides templated from polyethylene oxide surfactant assemblies. *Angew Chem Int Ed.* 2003;42:2872–2875.
21. Deng WH, Toepke MW, Shanks BH. Surfactant-assisted synthesis of alumina with hierarchical nanopores. *Adv Funct Mater.* 2003;13:61–65.
22. Zeng TY, Zhou ZM, Cheng ZM, Yuan WK. Effect of surfactant on the physical properties of hierarchically macro-mesoporous metal oxides. *Chem Lett.* 2010;39:680–681.
23. Joyal CLM, Butt JB. Chemisorption and disproportionation of carbon monoxide on palladium/silica catalysts of differing percentage metal exposed. *J Chem Soc Faraday Trans 1.*1987;83:2757–2764.
24. Collins A, Carriazo D, Davis SA, Mann S. Spontaneous template-free assembly of ordered macroporous titania. *Chem Commun.* 2004;568–569.
25. Deng WH, Shanks BH. Synthesis of hierarchically structured aluminas under controlled hydrodynamic conditions. *Chem Mater.* 2005; 17:3092–3100.
26. Hakim SH, Shanks BH. A comparative study of macroporous metal oxides synthesized via a unified approach. *Chem Mater.* 2009;21: 2027–2038.
27. Ren TZ, Yuan ZY, Su BL. Microwave-assisted preparation of hierarchical mesoporous-macroporous boehmite AlOOH and γ-Al_2O_3. *Langmuir.* 2004;20:1531–1534.
28. Anderson JR, Pratt KC. Introduction of Characterization and Testing of Catalysts. London: Academic Press Inc., 1985, Chapter 2.
29. Doğu T. Diffusion and reaction in catalyst pellets with bidisperse pore size distribution. *Ind Eng Chem Res.* 1998;37:2158–2171.
30. Silva VMTM, Rodrigues AE. Adsorption and diffusion in bidisperse pore structures. *Ind Eng Chem Res.* 1999;38:4023–4031.
31. Delgado JA, Rodrigues AE. A Maxwell-Stefan model of bidisperse pore pressurization for Langmuir adsorption of gas mixtures. *Ind Eng Chem Res.* 2001;40:2289–2301.
32. Nir A, Pismen LM. Simultaneous intraparticle forced convection, diffusion and reaction in a porous catalyst. *Chem Eng Sci.* 1977; 32:35–41.
33. Rodrigues AE, Ahn BJ, Zoulalian A. Intraparticle-forced convection effect in catalyst diffusivity measurements and reactor d esign. *AIChE J.* 1982;28:541–546.
34. Leitão A, Rodrigues AE. The influence of intraparticle convection on product distribution for series-parallel catalytic reactions. *Trans IChemE.* 1995;73A:130–135.
35. Leitão A, Rodrigues AE. Catalytic processes using "large-pore" materials: effects of the flow rate and operating temperature on the conversion in a plug-flow reactor for irreversible first-order reactions. *Chem Eng J.* 1995;60:111–116.
36. Rosenbrock HH, Storey C. *Computational Techniques for Chemical Engineers*. New York: Pergamon, 1966.
37. Petzold LR. A description of DASSL: a differential/algebraic system solver. Report SAND82–8637, Albuquerque, NM: Sandia National Laboratories, 1982.
38. Brenan KE, Campbell SL, Petzold LR. *Numerical Solution of Initial-Value Problems in Differential-Algebraic Equations.* New York: North-Holland, 1989.
39. Froment GF, Bischoff KB. *Chemical Reactor Analysis and Design, 2nd ed.* New York: Wiley, 1990.
40. Fillion B, Morsi BI, Heier KR, Machado RM. Kinetics, gas-liquid mass transfer, and modeling of the soybean oil hydrogenation process. *Ind Eng Chem Res.* 2002;41:697–709, 3052.
41. Chaudhari RV, Jaganathan R, Kolhe DS, Emig G, Hofmann F. Kinetic modelling of a complex consecutive reaction in a slurry reactor: hydrogenation of phenyl acetylene. *Chem Eng Sci.* 1986;41: 3073–3081.
42. Jackson SD, Shaw LA. The liquid-phase hydrogenation of phenyl acetylene and styrene on a palladium/carbon catalyst. *Appl Catal A: Gen.* 1996;134:91–99.

Manuscript received July 12, 2010, and revision received Aug. 23, 2010.